CrystEngComm

COMMUNICATION

View Article Online
View Journal | View Issue

Cite this: *CrystEngComm*, 2025, **27**, 6122

Received 16th July 2025,
Accepted 1st September 2025

DOI: 10.1039/d5ce00709g

rsc.li/crystengcomm

Effect of electrochemically active surface area on the charge-transfer resistance of layered positive electrode materials

Kingo Ariyoshi *[a] and Toshiyuki Tanaka[b]

Clarifying the relationship between the electrochemically active surface area and power capability is important for producing high-power batteries. In this study, the impact of particle morphology on the electrochemical kinetics of $LiNi_{1/3}Co_{1/3}Mn_{1/3}O_2$ (NCM) materials was investigated *via* rate-capability tests and electrochemical impedance spectroscopy using diluted NCM electrodes. In particular, different sizes and shapes of NCM materials were compared. The rate capability was governed by the particle size and shape, which were correlated with the Li-ion diffusion length and electrochemically active surface area. In addition, charge-transfer resistance was inversely proportional to the electrochemically active surface area, highlighting the importance of facet engineering. Therefore, optimising the particle morphology to selectively enhance active surfaces supports high-power and high-rate capabilities.

Li-ion batteries (LIBs) have recently been used in electric vehicles owing to their high energy density, and their evolution is essential for improving the performance of electric vehicles. To reduce the charging time and enhance regenerative performance, the power capability of LIBs can be improved by decreasing electrode resistance. Nanosized electrode materials have been extensively investigated because nanoparticles possess large surface areas for electrochemical reactions.[1] However, their large specific surface area also promotes side reactions, such as material dissolution, electrolyte decomposition, and solid–electrolyte interphase formation; therefore, nanosizing alone cannot realise both high power and long life.

Because power capability is closely related to the crystal orientation of the thin-film electrode in layered $LiCoO_2$ materials,[2,3] power capability (W g^{-1}) should be related to the electrochemically active surface area of the active material. Moreover, rate capability is related to the particle size and shape. For example, Li-ion diffusion within particles depends on the current density per electrochemically active surface area and diffusion distance. Consequently, the electrochemical activity of layered materials depends on the crystal facets. The cyclability of layered materials is also related to particle morphology.[4–6] Considering these phenomena, the electrochemical properties of a material are dependent on particle morphology.

To overcome the trade-off between rate and power capabilities and structural stability, particle morphology modulation can be used to increase the surface area. This approach can enhance power capability by increasing the active surface area of the material while maintaining total surface area. To validate this approach, the quantitative correlation between the surface area of the specific crystal facets of $LiNi_{1/3}Co_{1/3}Mn_{1/3}O_2$ (NCM) and its power and rate capabilities was determined. Clarifying the relationship between the electrochemically active surface area and power capability is extremely significant, both from the academic perspective of establishing the kinetics of the Li insertion reaction and from the engineering perspective of providing effective guidelines for electrode materials for high-power batteries.

In this study, we investigated the relationship between the particle morphology of NCM and electrochemical reaction kinetics with regard to the electrochemically active surface area. To measure the essential properties of the NCM materials, we conducted rate capability tests and electrochemical impedance spectroscopy using the diluted-electrode method.[7–12] Similar to thin-film and single-particle electrodes, the diluted electrode enabled the evaluation of the intrinsic electrochemical properties of materials, because a small amount of active-material particles is homogenously distributed in the diluted electrode (Fig. S1). The procedures for electrode preparation and cell fabrication are presented in the SI. Four types of NCM particles (small/large and plate-

[a] *Department of Chemistry and Bioengineering, Graduate School of Engineering, Osaka Metropolitan University, Sumiyoshi, Osaka 558-8585, Japan.*
E-mail: ariyoshi@omu.ac.jp
[b] *Department of Chemistry and Bioengineering, Graduate School of Engineering, Osaka City University, Sumiyoshi, Osaka 558-8585, Japan*

like/octahedral crystals) were synthesised using flux methods[13] and employed as active materials (Fig. S2). The NCM particles exhibited a layered structure with the same lattice parameters (a = 2.86 Å, c = 14.2 Å). The electrochemical behaviour of the NCM particles, which were examined in Li cells (Fig. S2), was similar to that previously reported.[14,15] For example, they exhibited an operating voltage of 4 V, with approximately 120 mAh g^{-1} of rechargeable capacity.

To determine the conditions of a suitable diluted electrode for evaluating the electrochemical properties of NCM, rate capability tests were performed using diluted electrodes with various NCM contents (Fig. S3). The contents of active NCM material in these diluted electrodes were 20, 10, and 5 wt%. When the NCM content was low, the discharge capacity increased, particularly at a high current density. According to the capacity retention *versus* current density plots based on NCM weight (Fig. S4), capacity retention improved as the NCM content decreased. However, it remained the same at NCM contents of <10 wt%. Thus, solid-state Li-ion diffusion inside the NCM particles was the rate-determining step. The amount of Li ions in the electrolyte required for the Li insertion reaction was sufficient owing to the low number of NCM particles in the diluted electrode.[7,9] Consequently, we used diluted electrodes containing 10 wt% NCM to evaluate the rate capability of NCM materials with solid-state Li-ion diffusion as the rate-determining step.

To examine the impact of particle morphology on the rate capability of NCM, the diluted NCM electrodes containing 10 wt% NCM with various particle shapes and sizes were discharged at several current densities (Fig. 1). For all cells, changes in the discharge curves with increasing current density were similar; however, the current density required to deliver the same capacity was significantly different. When comparing the rate capabilities of NCM with different particle sizes, smaller NCM particles exhibited better rate capability. For example, to deliver 80 mAh g^{-1}, the current densities were 1010 and 136 mA g^{-1} for the small and large octahedral crystals, respectively. Notably, the rate capabilities of the plate-like and octahedral crystals were similar. For example, for large crystals, the current density was 260 mA g^{-1} to deliver 60 mAh g^{-1}. Thus, particle size more significantly affected the rate capability of NCM than did particle shape.

Differences in the rate capabilities of NCM materials with different particle morphologies were examined by plotting capacity retention against the current density based on NCM weight (Fig. S5). The rate capabilities of the four NCM materials differed at high current densities but were similar at low current densities. The capacity retention of NCM materials with layered structures was proportional to the square root of the current density (Fig. S6). Conversely, in other materials with spinel structures, the capacity retention is proportional to the current density.[7,9,12] As shown in Fig. S5 and S6, small crystals exhibited better rate capabilities than large crystals for both octahedral and plate-like NCM materials. However, no significant difference was observed in the rate capabilities of the plate-like and octahedral crystals. When the particles were large, the plate-like and octahedral NCM materials exhibited similar rate capabilities. Conversely, when the particles were small, the rate capability of the octahedral crystals was slightly superior to that of the plate-like crystals. Thus, the rate capability of NCM was more significantly affected by particle size than by particle shape because the rate capability measured using the diluted electrodes was strongly correlated to the diffusion length of the particles.[11]

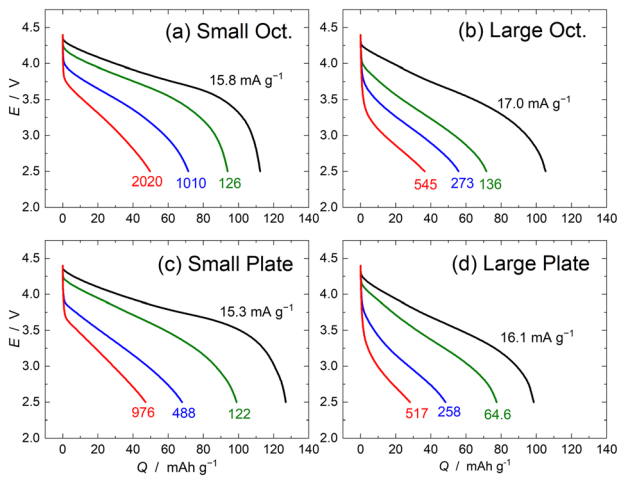

Fig. 1 Discharge curves during the rate capability tests of diluted NCM electrodes containing 10 wt% NCM. Morphology of NCM: (a) small octahedral, (b) large octahedral, (c) small plate-like, and (d) large plate-like particles.

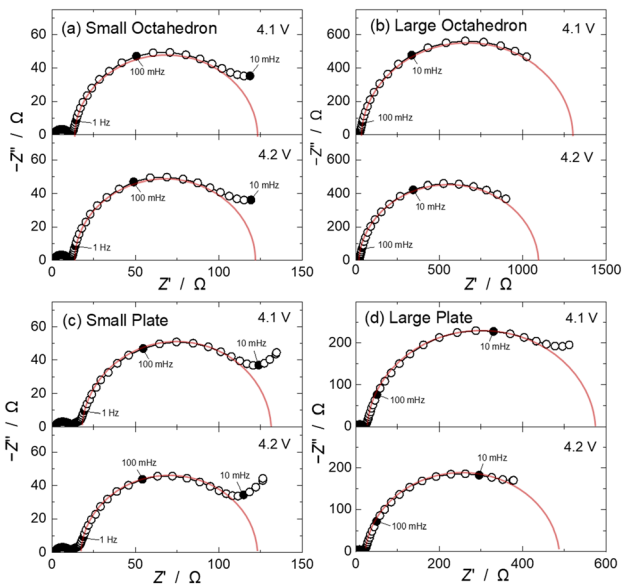

Fig. 2 Nyquist plots of Li/NCM cells measured at 4.1 and 4.2 V. The diluted NCM electrodes contained 10 wt% NCM. Morphologies of NCM: (a) small octahedral, (b) large octahedral, (c) small plate-like, and (d) large plate-like particles.

Electrochemical impedance measurements were performed to investigate the impact of particle morphology on the Li insertion kinetics of the NCM materials. In the Nyquist plots of diluted NCM electrodes measured at 4.1 and 4.2 V (Fig. 2), a large arc appeared in the low-frequency region, and a small arc was observed in the high-frequency region. According to previous studies,[8,10,16–20] the high-frequency arc is attributed to contact resistance between the active material and current collector, while the low-frequency arc corresponds to the charge-transfer resistance (R_{ct}) of the particles. In the diluted electrode with a low NCM content (10 wt%), the total surface area of the NCM particles in the electrodes was small owing to the low number of NCM particles; thus, the low-frequency arc due to R_{ct} increased in size. The R_{ct} value, which was estimated from the diameter of the low-frequency arc, increased with particle size for both plate-like and octahedral crystals, because larger crystals have a smaller surface area.[10] No significant difference in R_{ct} value was observed between 4.1 and 4.2 V. Therefore, the measured R_{ct} value can be used to evaluate the electrochemical properties of NCM materials, despite certain variations in NCM materials with a layered structure depending on the state-of-charge.[20,21]

To clarify the reason for significant differences in the R_{ct} values of NCM depending on the particle morphology, we considered differences in the electrochemically active surface area (A_{active}) due to particle shape and size (Fig. 3).[2,3,6] The (100) planes, which are the sides of plate-like crystals, are electrochemically active because they contain Li-ion conduction paths. However, the (003) planes, which are the top and bottom surfaces of plate-like crystals, are electrochemically inactive because the Li insertion reaction is blocked by transition-metal ions. Therefore, only the sides of plate-like crystals are electrochemically active. In the octahedral crystal, six crystal faces, including the {012} and {110} faces, contain Li-ion conduction paths among all crystal faces on which oxide ions are closely packed; thus, these crystal faces are electrochemically active. However, the other two faces of {003} are electrochemically inactive because the conduction paths are filled with transition-metal ions. Therefore, only six of the eight crystal faces participate in this reaction. The A_{active} values were calculated for the octahedral and plate-like crystals, as shown in Table 1 and the SI.

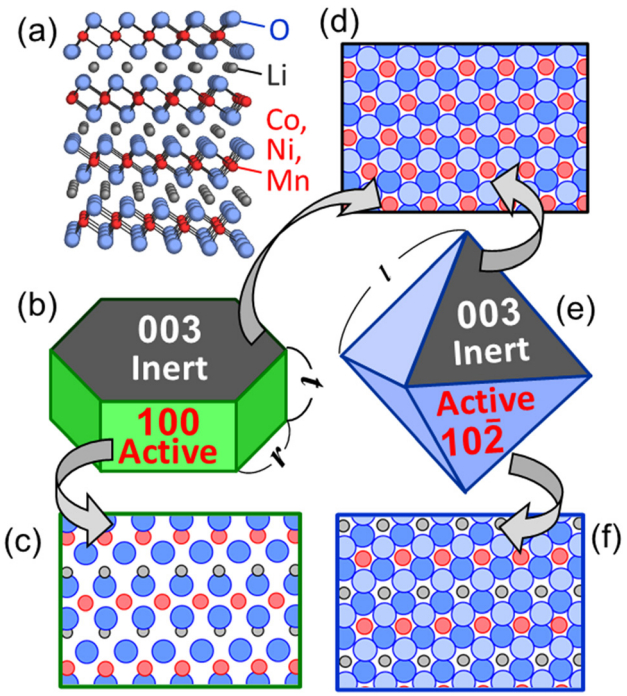

Fig. 3 (a) Crystal structure of NCM. (b and e) Miller indices of hexagonal plate and octahedral NCM crystals. Atomic arrangements of each crystal facet: (c and f) electrochemically active and (d) inactive surfaces.

To confirm that NCM with a larger A_{active} exhibits a lower R_{ct}, R_{ct} was plotted against A_{active} (Fig. 4a). To normalise the R_{ct} based on the NCM content, specific R_{ct} (Ω g) was calculated using the R_{ct} of the electrode multiplied by the NCM mass, because the R_{ct} of electrodes is inversely proportional to the NCM content. A linear relationship was observed in the plot of $\log R_{ct}$ *versus* $\log A_{active}$. The slope of the straight line was −1.0, suggesting that R_{ct} is inversely proportional to the A_{active} of NCM particles. Although a large error in the A_{active}, particularly for large crystals, was observed, the reciprocal of R_{ct} was proportional to A_{active}, and a straight line passing through the origin was drawn (Fig. S7). From the slope of this line, the R_{ct} per unit area of the electrochemically active surface in NCM was 8.4 kΩ cm^2. For the first time, we quantitatively clarified that only the electrochemically active crystal plane contributes to particle reactions of the Li insertion material. By controlling the particle morphology to selectively increase the electrochemically active surface area rather than reduce the particle size of Li insertion materials, we designed a highly durable material that achieves a high-power capability while suppressing side reactions on the surface.

Similar to the analysis of R_{ct} values, the relationship between rate capability and active surface area was examined (Fig. S8). The current density at which half of the discharge capacity can be obtained ($j_W@Q$ = 50%) was used as a quantitative index of rate capability. A linear relationship between $j_W@Q$ = 50% *versus* A_{active} in both octahedral and plate-like NCM crystals was observed. This relationship resulted from the dependence of current density on the active surface area; thus, the current density per active surface area decreased with increasing A_{active}. However, different particle

Table 1 A_{active} and R_{ct} values of the four types of NCM materials

	Small Oct.	Large Oct.	Small plate	Large plate
l or r [μm]	1.0	12	0.6	3.0
$A_{active} \times 10^{-4}$ [cm^2 g^{-1}]	1.2	0.096	0.80	0.16
d [μm]	0.36	4.3	0.52	2.6
R_{ct}@4.1 V [Ω g]	0.77	9.0	0.88	3.8
R_{ct}@4.2 V [Ω g]	0.76	7.6	0.79	3.3

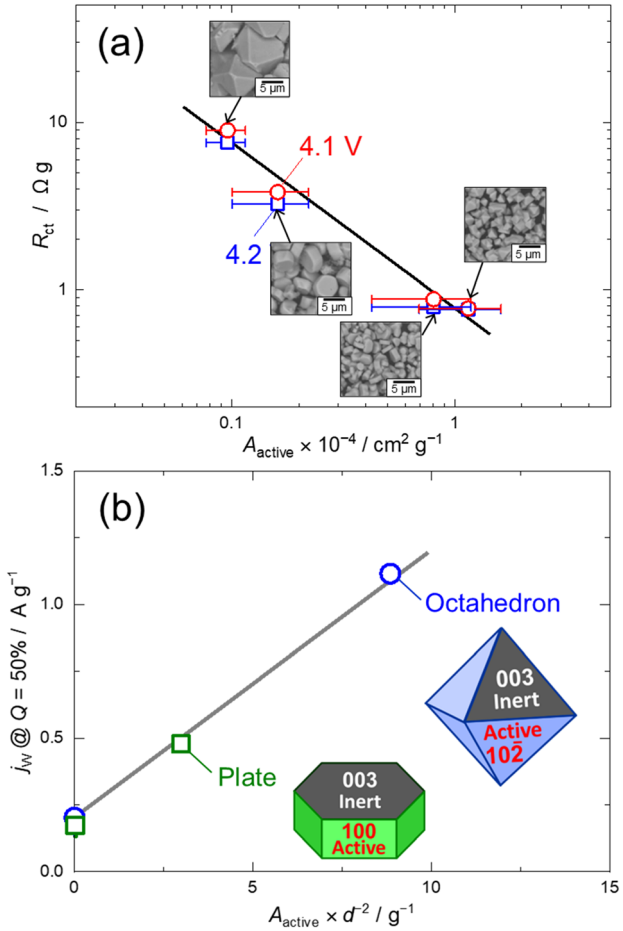

Fig. 4 (a) Plots of R_{ct} *versus* A_{active} in double-logarithmic scales. Red and blue symbols indicate R_{ct} measured at 4.1 and 4.2 V, respectively. (b) Plots of j_W@Q = 50% *versus* A_{active} × d^{-2}. Blue and green symbols represent octahedral and plate-like NCM particles, respectively.

shapes yielded straight lines with distinct slopes because the rate capability was limited by Li-ion diffusion within the solid NCM particles. During this process, both the particle surface area and Li-ion diffusion length within the particles played critical roles.

The diffusion distances of plate-like and octahedral NCM particles were estimated (Fig. S9). In a layered structure, the Li-ion conduction path corresponds to the two-dimensional plane perpendicular to the [003] direction. For plate-like particles, the diffusion distance equals the length from the centre to the edge of the hexagonal plane. In contrast, the diffusion distance in octahedral particles can be calculated from a cross-section perpendicular to the (003) plane of the octahedron. When finite diffusion within the active material determines the rate capability, the discharge capacity is inversely proportional to the square of the diffusion distance.[22] Consequently, rate capability is proportional to A_{active} and inversely proportional to the diffusion distance (d).

To confirm this expectation, j_W@Q = 50% was plotted against A_{active} × d^{-2}, and a linear relationship was obtained regardless of particle shape (Fig. 4b). The diffusion distance of the octahedral NCM particles (0.36 l) was shorter than that of the plate-like particles (0.87 r). Thus, the diffusion distance of plate-like particles approximately equals the particle radius, whereas that of octahedral particles is less than half the particle radius. For Li insertion materials, the same relationship between NCM crystals with different shapes demonstrated that the diffusion distance and active surface area played critical roles in determining the rate capability.

In summary, the dependence of Li insertion kinetics on the particle morphology of NCM materials with different particle shapes and sizes was investigated *via* rate capability tests and electrochemical impedance spectroscopy using the diluted-electrode method. Both particle shape and size played important roles on two different aspects of Li insertion kinetics: power and rate capabilities. Electrochemical impedance measurements revealed that power capability, which was evaluated using the R_{ct} value, was related to both the particle size and shape (plate-like/octahedral). For example, R_{ct} was significantly higher for larger particles and higher for octahedral crystals than for plate-like crystals. To quantitatively explain this difference, the A_{active} values of the four types of NCMs were calculated, and their relationship with R_{ct} was examined. The reciprocal of R_{ct} was proportional to A_{active}. Thus, R_{ct} was 8.4 kΩ cm^2 based on the active surface area of the NCM particles.

In addition to power capability, rate capability is closely related to particle size and shape. The electrochemically active surface area and diffusion distance strongly depend on particle morphology. Because layered materials contain two-dimensional Li-ion conduction paths, the diffusion distance within the particle varies depending on the particle shapes. Octahedral crystals have a shorter diffusion distance than plate-like crystals, even with the same particle size. This study demonstrates that modulating particle morphology while increasing the electrochemically active surface area and reducing the diffusion distance is an effective approach to enhance the power and rate capabilities of Li insertion materials.

Conflicts of interest

There are no conflicts to declare.

Data availability

Supplementary information: Experimental section; estimation of the surface area; characterization of NCM; SEM of a diluted electrode; discharge curves of diluted electrodes; capacity retention of diluted electrodes; capacity retention of NCM electrodes; plots of the reciprocal of R_{ct} against surface area; plots of the current density against surface area; diffusion distance of NCM particles. See DOI: **https://doi.org/10.1039/D5CE00709G**.

The data supporting this article have been included as part of the SI.

Acknowledgements

This work was supported by a grant from the GteX Program Japan (JPMJGX23S5) and JSPS KAKENHI (JP25K08317).

References

1 P. G. Bruce, B. Scrosati and J. M. Tarascon, *Angew. Chem., Int. Ed.*, 2008, **47**, 2930–2946.
2 P. J. Bouwman, B. A. Boukamp, H. J. M. Bouwmeester and P. H. L. Notten, *Solid State Ionics*, 2002, **152–153**, 181–188.
3 A. Yano, K. Hikima, J. Hata, K. Suzuki, M. Hirayama and R. Kanno, *J. Electrochem. Soc.*, 2018, **165**, A3221–A3229.
4 J. Zhu and G. Chen, *J. Mater. Chem. A*, 2019, **7**, 5463–5474.
5 F. Zou, J.-B. Kim, J. Zhang, G.-H. Lee, L. Lyu, J.-H. Choi, T. Kankaanpa, Y. M. Lee and Y.-M. Kang, *Energy Environ. Sci.*, 2024, **17**, 4319–4326.
6 C. Zhang, H. Dong, X. Zhang, J. Ye, Y. Zhan, P. Li, Y. Weng, B. Gu, G. Huang and S. Xu, *Chem. Eng. J.*, 2024, **502**, 158153.
7 K. Ariyoshi, S. Mizutani, T. Makino and Y. Yamada, *J. Electrochem. Soc.*, 2018, **165**, A3965.
8 K. Ariyoshi, S. Mizutani and Y. Yamada, *J. Power Sources*, 2019, **435**, 226810.
9 K. Ariyoshi, J. Sugawa and S. Masuda, *J. Electrochem. Soc.*, 2020, **167**, 140517.
10 K. Ariyoshi, M. Tanimoto and Y. Yamada, *Electrochim. Acta*, 2020, **364**, 137292.
11 K. Ariyoshi, J. Sugawa and S. Masuda, *J. Power Sources*, 2021, **509**, 230349.
12 K. Ariyoshi and J. Sugawa, *Electrochim. Acta*, 2023, **455**, 142425.
13 K. Ariyoshi and T. Tanaka, *Cryst. Growth Des.*, 2024, **24**, 3771–3776.
14 T. Ohzuku and Y. Makimura, *Chem. Lett.*, 2001, **30**, 642–643.
15 N. Yabuuchi and T. Ohzuku, *J. Power Sources*, 2003, **119**, 171–174.
16 N. Ogihara, S. Kawauchi, C. Okuda, Y. Itou, Y. Takeuchi and Y. Ukyo, *J. Electrochem. Soc.*, 2012, **159**, A1034–A1039.
17 H. Nara, D. Mukoyama, R. Shimizu, T. Momma and T. Osaka, *J. Power Sources*, 2019, **409**, 139–147.
18 A. S. Keefe, S. Buteau, I. G. Hill and J. R. Dahn, *J. Electrochem. Soc.*, 2019, **166**, A3272–A3279.
19 L. Stolz, M. Gaberšček, M. Winter and J. Kasnatscheew, *Chem. Mater.*, 2022, **34**, 10272–10278.
20 K. Ariyoshi, *Electrochemistry*, 2024, **92**, 37007.
21 H. Zhou, J. Izumi, S. Asano, K. Ito, K. Watanabe, K. Suzuki, F. Nemoto, N. L. Yamada, K. Aso, Y. Oshima, R. Kanno and M. Hirayama, *Adv. Energy Mater.*, 2023, **13**, 2302402.
22 K. Ariyoshi and J. Sugawa, *Electrochemistry*, 2021, **89**, 157–161.

